Faraday Discussions

Accepted Manuscript

This manuscript will be presented and discussed at a forthcoming Faraday Discussion meeting. All delegates can contribute to the discussion which will be included in the final volume.

Register now to attend! Full details of all upcoming meetings: http://rsc.li/fd-upcoming-meetings

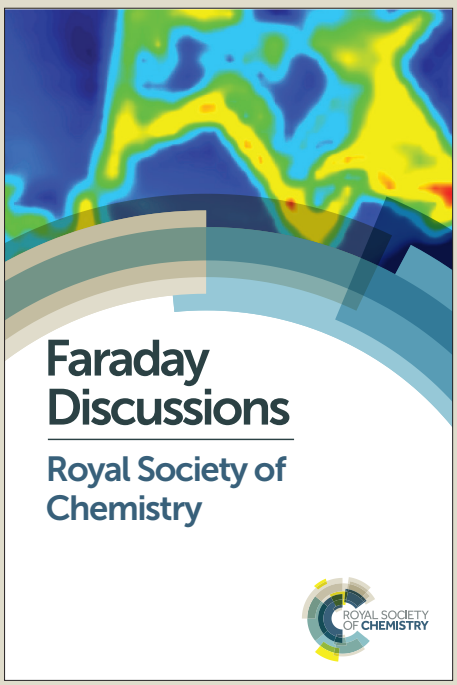

This is an *Accepted Manuscript*, which has been through the Royal Society of Chemistry peer review process and has been accepted for publication.

Accepted Manuscripts are published online shortly after acceptance, before technical editing, formatting and proof reading. Using this free service, authors can make their results available to the community, in citable form, before we publish the edited article. We will replace this *Accepted Manuscript* with the edited and formatted *Advance Article* as soon as it is available.

You can find more information about *Accepted Manuscripts* in the Information for Authors.

Please note that technical editing may introduce minor changes to the text and/or graphics, which may alter content. The journal's standard Terms & Conditions and the Ethical guidelines still apply. In no event shall the Royal Society of Chemistry be held responsible for any errors or omissions in this *Accepted Manuscript* or any consequences arising from the use of any information it contains.

ROYAL SOCIETY OF CHEMISTRY

www.rsc.org/faraday_d

The corrosion protection of AA 2024-T3 aluminium alloy by leaching of lithium-containing salts from organic coatings

Peter Visser*[a,c], Yanwen Liu[b], Xiaorong Zhou[b], Teruo Hashimoto[b], George E. Thompson[b], Stuart B. Lyon[b], Leendert G.J. van der Ven[c], Arjan J.M.C. Mol[a], Herman. A. Terryn[a, d]

DOI: 10.1039/b000000x [DO NOT ALTER/DELETE THIS TEXT]

Lithium carbonate and lithium oxalate were incorporated as leachable corrosion inhibitors in model organic coatings for the protection of AA2024-T3. The coated samples were artificially damaged with a scribe. It was found that the lithium-salts are able to leach from the organic coating and form a protective layer in the scribe on AA2024-T3 under neutral salt spray conditions. The present paper shows the first observation and analysis of these corrosion protective layers, generated from lithium-salt loaded organic coatings. The scribed areas were examined by scanning and transmission electron microscopies before and after neutral salt spray exposure (ASTM-B117). The protective layers typically consist of three different layered regions, including a relatively dense layer near the alloy substrate, a porous middle layer and a flake-shaped outer layer, with lithium uniformly distributed throughout all three layers. Scanning electron microscopy and white light interferometry surface roughness measurements demonstrate that the formation of the layer occurs rapidly and, therefore provides an effective inhibition mechanism. Based on the observation of this work, a mechanism is proposed for the formation of these protective layers.

1 Introduction

The development of alternative surface pretreatments and pigmented coatings to eliminate the health hazards and toxicity of soluble hexavalent chromium is being pursued for many years. Especially in the aeronautical industry, the replacement or elimination of hexavalent chromium has been and still is a major challenge.[1] High strength aluminium alloys such as AA2024-T3 and AA7075-T6 are most commonly used in aircraft design because of their favourable strength to weight ratio. However, these alloys are very susceptible to localized corrosion such as pitting and

[a] *Delft University of Technology, Department of Materials Science and Engineering, Delft, The Netherlands*
[b] *School of Materials, The University of Manchester, Manchester, UK.*
[c] *AkzoNobel, Automotive and Aerospace Coatings, Sassenheim, The Netherlands.*
[d] *Vrije Universiteit Brussel, Group of Electrochemistry and Surface Engineering, Brussels, Belgium*

intergranular corrosion.[2-4] For decades, chromate-containing organic coatings and chromate-based conversion coatings have been used for the protection of these high strength aluminium alloys, with superior performance. The corrosion protective scheme employs chromate in many steps, including pre-cleaning,[5] conversion coating/anodizing,[6-8] and the organic coatings.[9] These chemical conversion coatings and organic coatings provide active corrosion inhibition toward the substrate and have the ability to release hexavalent chromium in the case of a local defect to provide the "self-healing" protection.[10, 11] The unique properties of hexavalent chromium make the replacement of chromate inhibitor pigments in organic coatings a difficult task.[9, 12] Numerous investigations have been performed to find promising candidates to replace chromates in organic coatings. Ideally, these compounds should have a similar performance as chromates, i.e. providing corrosion protection to the substrate and serving as a reservoir of corrosion inhibitor, which has the ability to be released from the coating when damages occur and heal the defect by the formation of a protective or passivation layer.[13, 14] This leaching of soluble chemical species is the main corrosion inhibiting strategy used in corrosion inhibiting coating technology for the protection of high strength aluminium alloys.

Over the last few years, several inhibitors have been identified as promising replacement for chromates. These include oxo-anionic, cationic, metal, metal oxide, and organic inhibitors. The oxo-anionic inhibitor salts include molybdates,[15] metavanadates,[16, 17] permanganate,[18] and phosphates,[19-21] The cationic inhibitors include rare-earth compounds[22] such as cerium[23] and praseodymium.[24] Magnesium[25] and zinc[26] metals are also found to be effective when used as pigments in organic coatings. Furthermore, several organic inhibitors have shown promising results.[27-29] Whilst many approaches have been attempted to achieve acceptable alternatives, relatively few systems have demonstrated similar effectiveness as chromate containing systems.[30] Therefore, the search for suitable alternatives for chromates is continuing.

Recently, the use of lithium salts has been proposed as a potential replacement for chromate in organic coatings.[31] In the 1990s, alkaline lithium solutions have been studied as possible replacement of the traditional chromated chemical conversion process. Lithium salts, including lithium carbonate,[32-36] lithium sulphate,[32] lithium hydroxide[37] and lithium chloride[32] in aqueous alkaline environment have been shown to form a continuous polycrystalline layer on superpure aluminium,[33, 34] AA1100,[35, 36] AA6061,[32, 35] AA2024,[35, 37] and AA7075[35] aluminium alloys. The lithium-based conversion coating greatly increased the corrosion resistance of the various selected substrates by increasing the pitting potential and reducing the corrosion current density. The conversion coated superpure aluminium and AA6061 aluminium alloy passed the standard salt spray tests.[35] The protective properties provided by these lithium conversion layers are suggested to originate from the formation of a lithium-aluminium-hydroxide-carbonate-hydrate ($Li_2[Al_2(OH)_6]_2 \cdot CO_3 \cdot nH2O$) layer[35] with lithium aluminate as a pore filler.[34] Lithium is the only monovalent cation that is known to intercalate in aluminium hydroxide to form these layered double hydroxides.[38]

Although, lithium based chemical conversion layers have been studied using electrochemical approaches and corrosion tests, limited studies have been carried out with a focus on obtaining detailed morphological information, especially cross-sectional observation of the protective layer. Further, the mechanisms of layer formation remain unclear. Additionally, no detailed investigation has focused on the

use of lithium-containing species as leachable corrosion inhibitor incorporated into organic coatings.

In the present study, lithium-containing salts, i.e. lithium carbonate or lithium oxalate, were used as corrosion inhibitors in an organic model coating for the protection of AA2024-T3. The coatings were damaged and the scribe was examined by electron microscopic techniques, before and after exposure to the neutral salt spray corrosion test (ASTM B-117). This is the first investigation of such a protective layer that was generated on AA2024-T3, from an organic coating containing lithium–salt as leachable corrosion inhibitor. Specific and careful sample preparation combined with low-voltage scanning electron microscopy (SEM) cross-sectional work and high-resolution transmission electron microscopy (TEM) and electron energy loss spectroscopy (EELS) were used to reveal morphological and compositional information of the protective layer. In addition, the formation of the layer has been studied as a function of time by white light interferometry and cross-sectional SEM. A mechanism is proposed for the formation and the protective nature of this layer, based on the observations of this study.

2 Experimental

2.1 Materials

Model formulations based on polyurethane chemistry were designed using a polyester resin (Desmophen® MPA) and an aliphatic polyisocyanate (Tolonate® HDB 75 MX) with a NCO/OH ratio of 0.75 and a pigment volume concentration (PVC) of 30% as described in Table 1.

Tartaric-sulphuric acid (TSA) anodized AA2024-T3 unclad sheets were used as the substrate in this study (dimensions of 70 × 70 × 0.8 mm). The AA2024-T3 substrate (2024-T3 QQ-A250/5) was purchased from Alcoa and the TSA pretreatment was performed according to aerospace requirements (AIPI 02-01-003) at Premium AEROTEC, Bremen Germany.

Table 1 Composition of model organic coatings

	Supplier	Non-inhibiting	Lithium carbonate	Lithium oxalate
Component A				
N-Butylacetate	Sigma Aldrich	75.0 g	75.0 g	75.0 g
Desmophen 650MPA	Bayer Materials science	47.7 g	47.7 g	47.7 g
Lithium carbonate	Sigma Aldrich		23.6 g	
Lithium oxalate	Sigma Aldrich			32.0 g
Magnesium oxide	Sigma Aldrich		16.4 g	16.4 g
Tioxide TR 92	Huntsman		5.9 g	5.9 g
Blanc Fixe N ($Ba(SO_4)$)	Sachtleben		15.4 g	15.4 g
Component B				
Tolonate HDB 75 MX	Vencorex	28.5 g	28.5 g	28.5 g
Dynasilan Glymo	Evonik	5.2 g	5.2 g	5.2 g

2.2 Preparation and application of the model coating

The pigmented coatings were prepared according to the following procedure:
All components of Component A were added under stirring in a 370 ml glass jar. After addition of the final component, 400 grams of Zirconox® pearls (1.7 -2.4 mm) were added to the mixture. The pigments were dispersed to a particle size smaller than 25 μm by 20 minutes shaking on a Skandex® paint shaker. After this procedure, the mixtures were filtered to remove the pearls. The ingredients of component B were mixed separately.

Component B was added to Component A and the mixture was stirred to a homogeneous mixture. The paints were applied with a HVLP spray gun on the AA 2024 –T3 unclad TSA panels, 30 minutes after mixing. The coatings were cured at 80°C for 16 hours. The measured dry film thickness was 20-25 μm.

A mechanical milling device was used to artificially damage the coating with a U-shaped scribe, before exposing the samples to the neutral salt spray test (ASTM-B117). The panels were scribed from corner to corner, leaving a 1mm wide scribe that penetrated 100-150 μm deep into the metal.

2.3 Experimental techniques.

The samples were exposed to the Neutral Salt Spray (ASTM-B117) test for varying periods from 30 minutes up to 168 hours. After exposure, the process was quenched by a 2 minute rinse with flowing demineralised water to remove any residual chlorides and the panels were air dried.

Scanning Electron Microscopy (SEM)
The cross sectional observation of the oxide layers, in the scribe, was carried out by scanning electron microscopy (SEM) using a ZEISS Ultra 55 instrument with an acceleration voltage of 0.5 kV. The composition of the oxide films was analysed by energy dispersive X-ray analysis on FEI Magellan HR FEG-SEM.

Transmission electron microscopy *(TEM-EELS)*
The layers were also examined by transmission electron microscopy (TEM) using a JEOL FX 2000 II instrument operated at 120 kV, with a nominal sample thickness of 15 nm, prepared by a Leica EM UC6 ultra-microtome with a diamond knife. Electron energy loss spectroscopy (EELS) was conducted on a TECNAI TF30 TEM fitted with a Gif2001 detector, operated at 300 kV Mapping images were acquired with 1024×1024 pixels, this results pixel size of 0.56×0.56 nm for the selected magnification.

White light Interferometry (WLI)
The surface roughness of the scribe was measured with WLI, using a Veeco NT1100 profileometer. The high-resolution measurements were carried out using a 20x objective and multiple measurements were stitched together to sample a 2 mm length of the scribe. The data were de-trended by removal of any planar tilt. In order to remove the low frequency spatial waves associated with scribing a high pass Fourier filter was used with a frequency cut-off of 5 mm^{-1}. Visibly corroded samples were subjected to a cleaning step (1hour 1M Nitric acid) to dissolve the corrosion

products and reveal the attacked morphology of the substrate.

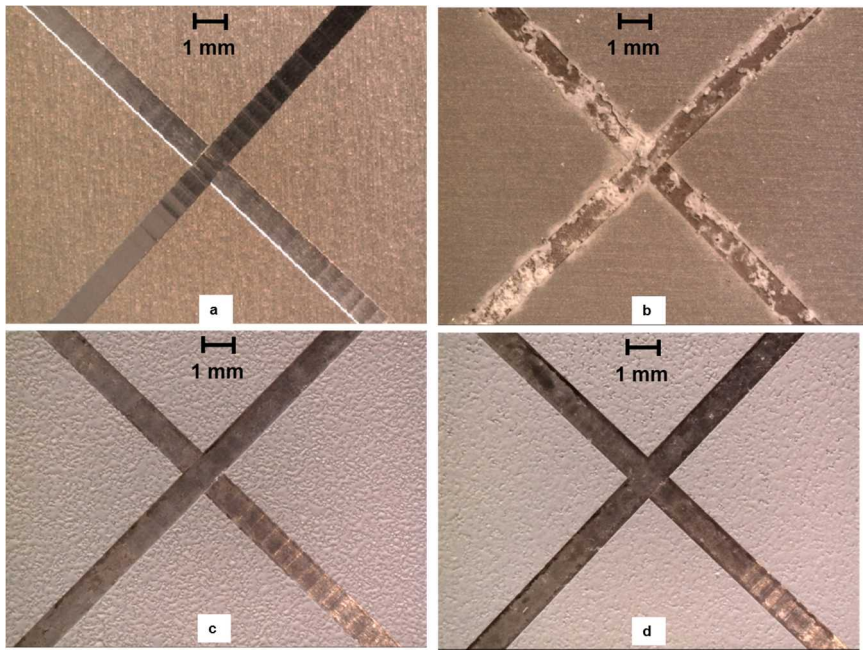

Fig. 1 Optical images of coated and scribed AA2024-T3 panels before and after 168 hours Neutral Salt Spray exposure (ASTM B-117) (a) unexposed (b) No inhibitor, (c) lithium carbonate, and (d) lithium oxalate.

3 Results and discussion

3.1 General morphological observations in the scribed area before and after salt spray testing

The scribed regions were examined with an optical microscope. Fig. 1a shows the scribe before exposure to the accelerated corrosion test. The pristine scribe is 1 mm wide and 100 μm deep into the alloy. The panels were exposed to 168 hours neutral salt spray (ASTM B-117). Fig. 1b shows the detrimental effect of the corrosive conditions when a coating does not contain an effective corrosion inhibitor. The coating remains intact but the scribe is heavily affected and contains many areas with white corrosion products. In contrast to this, the lithium-salt loaded coatings remained free of corrosion products (Fig. 1c-d). Both, lithium carbonate and oxalate show a similar protective behaviour. These lithium salts were selected for this study because of their moderate solubility compared to most other lithium salts, respectively 1.3 g/100 mL for lithium carbonate and 8 g/100 mL for lithium oxalate, and ease of paint formulation.

These observations and visual comparison of the scribed areas of coated AA2024-T3 before and after salt spray testing indicates the important role of the presence of lithium-containing salts as corrosion inhibitor in organic coatings, leading to a detailed investigation of the protection mechanism of the AA2024-T3 by lithium-containing salts, as discussed below.

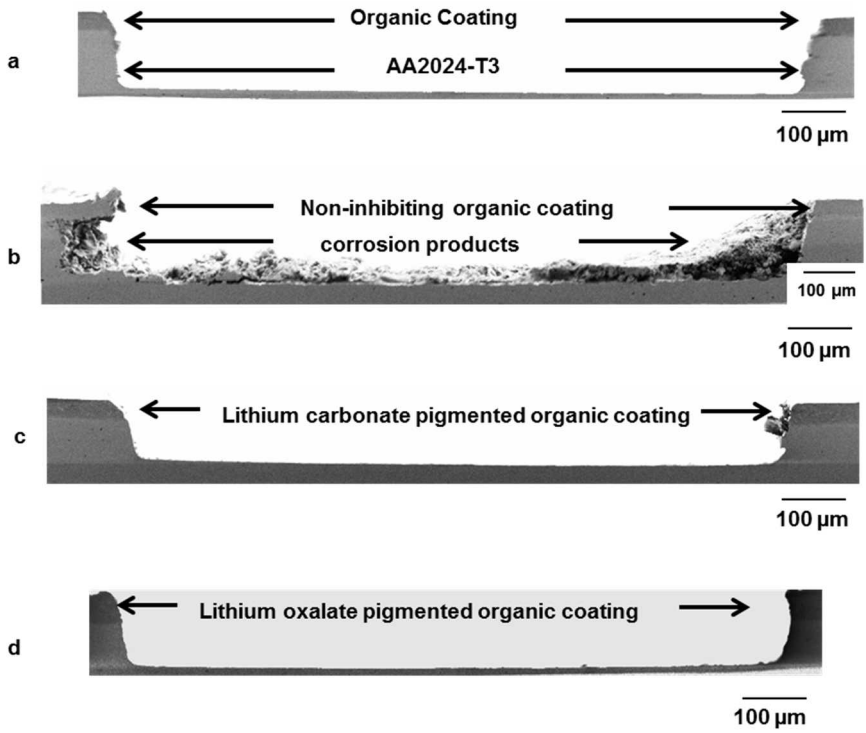

Fig. 2. Cross-section SEM images of coated and scribed AA2024-T3 panels before and after 168 hours Neutral Salt Spray exposure (ASTM B-117) (a) unexposed, (b) no inhibitor, (c) lithium carbonate, and (d) lithium oxalate.

3.2 Detailed morphological observations in the scribed area before and after salt spray testing

The scribed region was examined in more detail by studying cross-sections using scanning electron microscopy. The cross-sections of the scribed area of the alloy substrate showed a "U" shape in the middle of the images, with the organic coated alloy substrate evident on both sides (Fig. 2a). After 168 hours salt spray exposure, the scribed alloy with the non-inhibiting coating showed the presence of a large amount of corrosion products with a typical thickness about 25 µm (Fig. 2b). However, when lithium carbonate or lithium oxalate was incorporated as a corrosion inhibitor in the organic coating, no apparent damage is observed in the scribed area, as shown in Figs. 2c and 2d.

3.2.1 Non-inhibited coating

The scribed area of the non-inhibited coating has been examined after 168 hours neutral salt spray exposure. The SEM cross-section clearly showed the hydrated aluminium oxide formed during salt spray exposure; Fig. 3a displays the full scribe with the corrosion products. Fig. 3b shows the cross-section of the corrosion products at higher magnification, with pores providing access to the metal surface for aggressive ions. Although the metal/oxide or hydroxide interface is relatively flat, the corrosion products are homogeneously distributed in the scribe. Fig. 3a indicates a relatively uniform corrosion process. However, localised corrosion, such

as pitting and intergranular, was observed as well (Fig. 3c). It is evident that the grain boundary of the alloy is vulnerable to corrosion attack, especially when second phase particles are present at the grain boundaries. EDX analyses revealed that the corrosion products contained mainly aluminium and oxygen, with traces of copper and magnesium present.

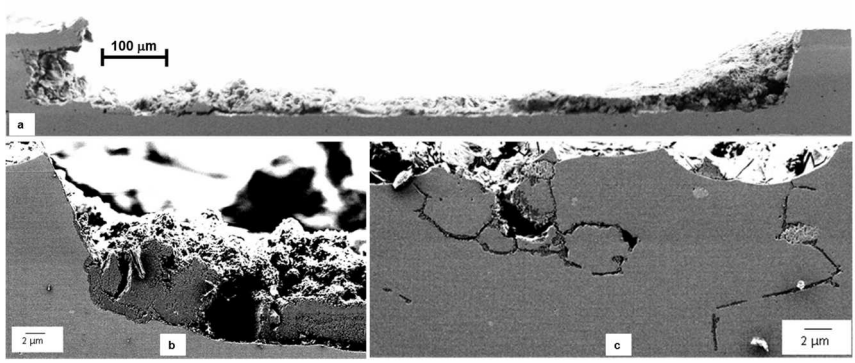

Fig. 3. SEM crosscut images of non-inhibited coating on AA2024 T3. (a) full scribe with corrosion products, (b) detailed corrosion products, (c) intergranular corrosion.

According to Foley,[39] corrosion of aluminium commences according to a multi-step process which leads to oxide thinning and finally dissolution of the aluminium. This dissolution is followed by a fast hydrolysis of the Al^{3+} ion to form $Al(OH)_3$ that transforms into $Al_2O_3 \cdot H_2O$. Further, EDX analyses of the corrosion products indicated that the corrosion products are mainly hydrated aluminium oxide ($Al_2O_3 \cdot H_2O$) or aluminium hydroxide ($Al(OH)_3$), with oxygen to aluminium ratios in the ranging from of 2:1 up to 4:1. This correlates with various hydrated aluminium oxides, which are common corrosion products of aluminium occurring in chloride containing solutions.[40]

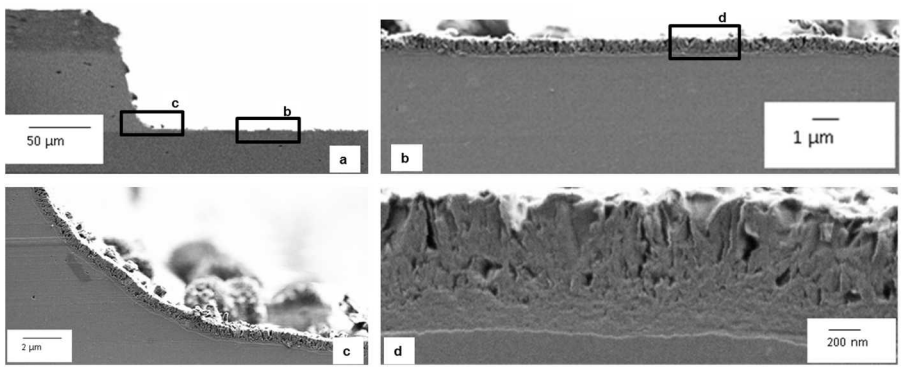

Fig. 4 SEM cross-cut images of protective layers generated from a lithium carbonate loaded coating after 168 hours ASTM B-117 exposure (a) scribed area, (b) middle section of the scribe, (c) curved area of bottom of the scribe , (d) detailed morphology of layer (middle section of the scribe).

3.2.2 Lithium-salt containing coatings

In contrast to the scribed area of the non-inhibited coating, the lithium-salt loaded organic coatings did not show this type of corrosion and the scribed areas were

without any significant amount of corrosion products after 168 hours neutral salt spray exposure. For both samples, SEM investigations reveal that the substrate of the scribe is covered with a new layer.

Fig. 4 shows the SEM cross-sectional examination of the protective layer generated from a lithium carbonate loaded coating. A thin deposited layer, of about 0.5 to 1.5 µm thickness, developed throughout the scribed surface area (Fig. 4 b and c). Higher magnification images reveal a typical detailed morphology of the layer formed (Fig. 4d). The layer comprises three distinct regions: a dense barrier region at the metal/deposited layer interface, a porous region in the middle, and a columnar outer region. This outer region can be correlated with the surface as observed with a planar view SEM image (Fig. 5c)

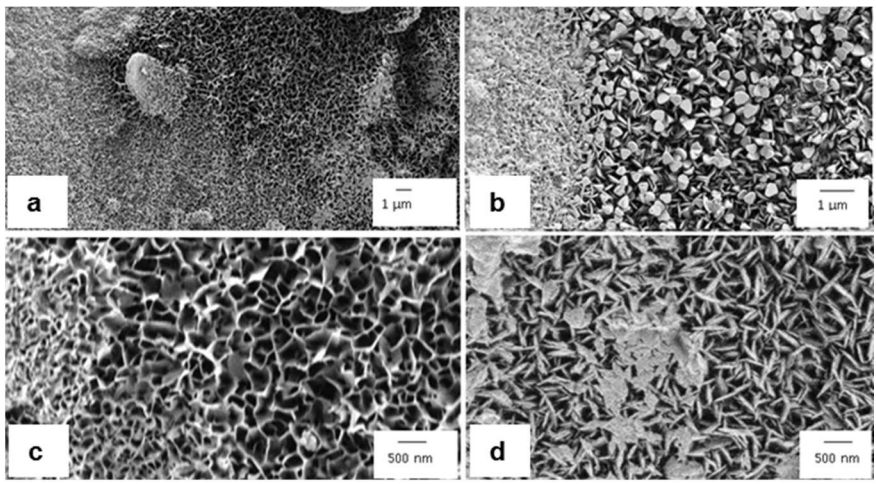

Fig. 5. Top view appearance of protective layer with increasing magnification after 168 hours ASTM B-117 exposure. (a), (c) lithium carbonate and (b), (d) lithium oxalate.

Fine textures were observed on the overall surface at increased magnification (Fig. 5c, d). Both the lithium carbonate and lithium oxalate pigmented primers show this particular textures. In some regions, the texture is more significant, while in other regions the surface is still relatively flat. The textures comprised fine flakes, with some oriented almost vertical to the surface (Fig. 5d) while others are randomly orientated. It is unclear whether this different top-view morphology or textures is a result of the anion or different lithium ion concentrations due to the higher solubility of lithium oxalate. This study did not focus on the anion effect. However, these observations justify further studies on the effect of the anion on the formation of these protective layers.

The lithium oxalate loaded model coating demonstrates similar deposition behaviour in the scribed region after salt spray testing (Fig. 6.). SEM cross-sectional examination revealed the same three distinct morphologies of a dense barrier region, porous region, and columnar outer region, similar to the deposited layer of the lithium carbonate sample. Although the flakes formed are finer and denser compared with the morphologies of the film formed from the coated alloy pigmented with lithium carbonate.

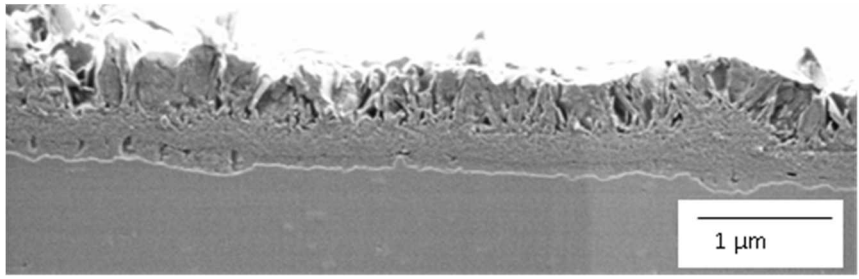

Fig. 6. SEM cross-sectional image of the typical morphology of the protective layer generated from a lithium oxalate loaded coating.

The observed inhibitive effect must be a result of this layer, which was generated in-situ in the damaged area. The presence of the columnar layer at the outer region of the cross-section and the microstructure of the surface could indicate the possible formation of a lithium–aluminium-carbonate-hydroxide hydrate as reported by Drewien *et al.*[36] They generated these protective poly-crystalline layers on aluminium from saturated aluminate ($Al(OH)_4^-$) alkaline lithium (pH 11.5-13) solutions under well-controlled conditions. Besides the poly-crystalline layer, a thin very fine or poorly crystalline layer was found underneath the poly-crystalline layer. However, the performance of these layers was not sufficient for the protection of AA2024-T3.

Layers with a similar morphology as found in this study, have been observed when exposing aluminium to (weak) alkaline solutions.[41, 42] The ratio of the thickness of the inner barrier layer versus the non-barrier outer layer was found to depend on the pH of the solution. It was suggested that the layer was initially formed by initially an aluminium hydroxide gel, which aged to boehmite and pseudoboemite and later to bayerite. However, these layers did not provide long-term corrosion protection.

The results from this study suggest that lithium-containing species in the organic coating provide fast and effective corrosion protection to the aluminium alloy. The layered morphology is significant different from the layers formed in the conversion process. The inhibitive properties of this layer might be derived from the presence of the dense non-porous layers near the aluminium substrate.

3.3 Composition of the protective layer

The composition of the deposited layer has been analysed with transmission electron microscopy equipped with electron energy loss spectroscopy (TEM-EELS) in order to detect the lithium species in the layer. The TEM image and corresponding EELS maps of the layer generated from the lithium carbonate based coating are shown in Fig.7 a-d. These maps demonstrated the presence of aluminium, oxygen, and lithium throughout the deposited layer. The bright regions in Fig.7d indicate the uniform distribution of lithium throughout the entire layer. Similar results were also obtained from the scribed area of the AA2024-T3 aluminium alloy with lithium oxalate pigmented coating. The TEM images showed the presence of the barrier film on metal surface followed by fine porous and flake network regions.

The presence of lithium throughout the protective layer including the dense layer shows that lithium-ions leached from the organic coating matrix into the scribe and formed a protective layer in the scribe that consists of lithium, aluminium and oxygen. Whereas the hydrated aluminium oxides of the non-inhibited sample are not

able to prevent the aluminium matrix from further dissolution and pitting corrosion, these results indicate that the morphology and composition of these lithium-based layers provide long-term corrosion protection.

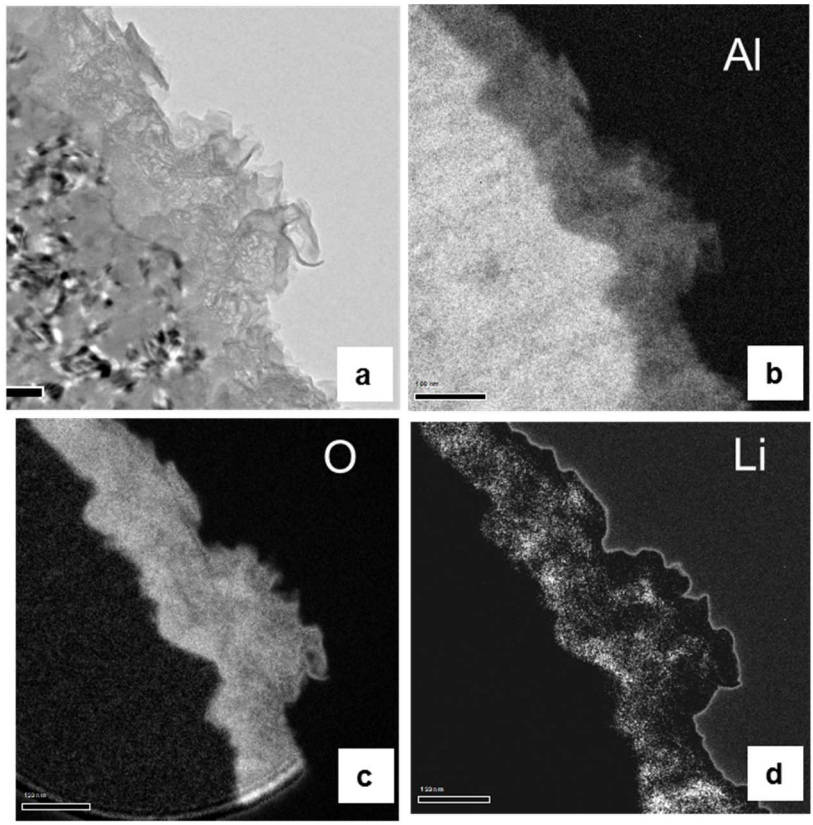

Fig.7 TEM image and TEM-EELS elemental mapping of the layer generated from the lithium carbonate loaded coating (a) TEM image, (b) Aluminium, (c) Oxygen, and (d) lithium distribution

3.4 Rate of the protective layer formation.

3.4.1 Surface roughness development in time.

White light interferometry (WLI) has been used to quantify the degree of corrosion by measuring the surface roughness (s_a) of the scribed areas after different periods of salt spray exposure. Figure 8 shows the development of the surface roughness of the samples over time when exposed to the corrosive salt spray conditions. An unexposed scribe has a typical surface roughness of about 170 nm (Fig. 9a).

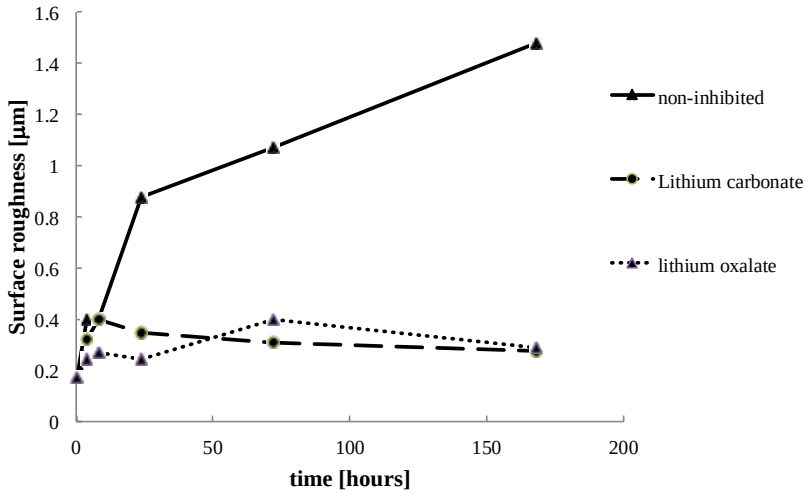

Fig. 8 Development of the surface roughness in the scribe measured by white light interferometry after different periods of neutral salt spray exposure.

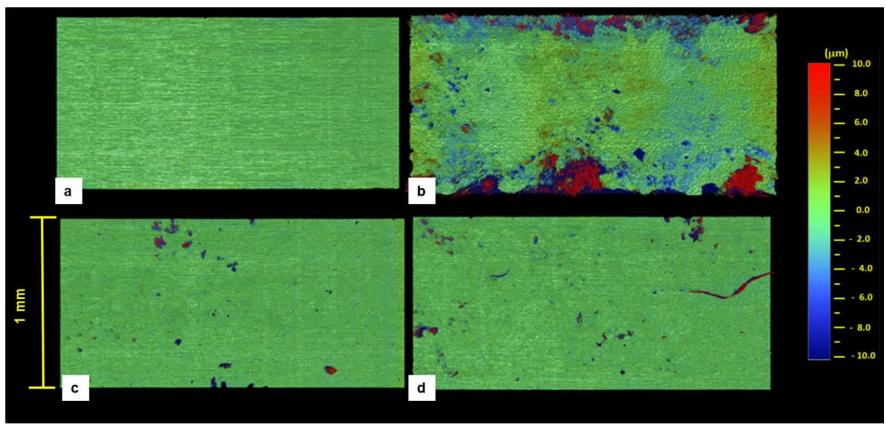

Fig. 9 High-resolution WLI images of the scribed area before and after 168 h exposure to neutral salt spray conditions, (a) unexposed scribe, (b) non-inhibited coating, (c) Lithium carbonate coating and, (d) lithium oxalate coating.

The detrimental effect of the corrosive conditions on the non-inhibiting sample is evident. The surface of the scribe is severely damaged due to pitting corrosion and the dissolution of aluminium. The surface roughness of the non-inhibiting sample increased rapidly after the aluminium oxide layer had been de-stabilised and localized corrosion processes were initiated. After 24 hours exposure the roughness increased up to 0.9 µm and this increased further to 1.5 µm after 168 hours. In contrast to this, the surface roughness of the lithium-salt containing coatings increased to 0.3-0.4 µm and remained relatively constant from then onwards. This demonstrates that slow or ineffective inhibition mechanisms result in rapid increase of the surface roughness in the scribe due to pitting corrosion and aluminium dissolution processes,[43] as illustrated for the non-inhibited sample in Fig 9b.

Compared to the unexposed sample, the WLI scan of non-inhibited sample visualizes the degree of damage caused by corrosion in the first 168 hours. On the other hand, the lithium-based samples show only limited pitting corrosion and a superficial attack on the surface which is illustrated by in Figs. 9 c and d. Therefore it can be concluded that the lithium-based coatings provide fast and effective inhibition on AA2024 –T3.

3.4.2 Generation of the protective layer

The WLI results indicate that the inhibition mechanism must be fast and complete within 48 hours. SEM crosscuts were made after 4 and 8 hours with the aim to observe the generation of the protective layer at an early stage.

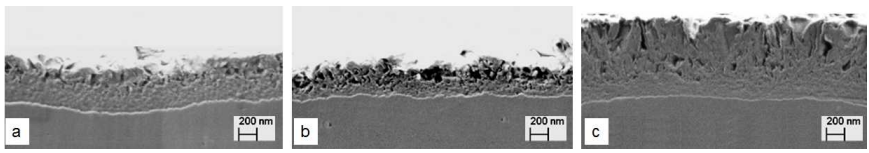

Fig. 10 SEM cross-cut images of the protective layer generated from the lithium carbonate loaded coating after (a) 4 hours, (b) 8 hours and, (c) 168 hours neutral salt spray conditions.

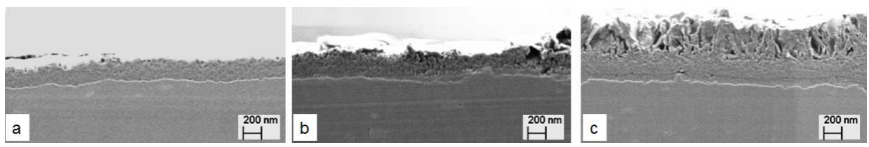

Fig. 11 SEM cross-cut images of the protective layer generated from the lithium oxalate loaded coating after (a) 4 hours, (b) 8 hours and, (c) 168 hours neutral salt spray conditions.

Figs. 10 and 11 show the formation of the protective layer after 4 and 8 hours neutral salt spray exposure. After 4 hours, both the lithium carbonate and lithium oxalate loaded coatings (Figs 10a and 11a) provide a protective layer with a thickness between 200 and 400 nm in the scribe. These layers have a similar morphology and thickness as the dense layers as found underneath the porous columnar layer after 168 hours exposure. After 4 and 8 hours, there is some columnar material present on top of the porous layer. According to these observations, it seems that the columnar layer is formed at a later stage in the process and increases the thickness of the protective layer to 1-1.5 μm.

3.5 Proposed mechanism of passive film formation

Lithium species have been leaching from the organic coating and a three-layered protective layer has been formed on AA2024-T3. However, the mechanism of the formation is not yet fully understood. SEM cross-sectional and TEM-EELS microscopic techniques have provided information about the protective layer in more detail. Based on this information a mechanism is proposed for the formation of such a layer.

The SEM-cross-sectional results reveal the significant different morphology for these layers compared to the poly-crystalline layers generated at high pH and saturated aluminate solutions in the chemical conversion process of Drewien *et al.*[36] This can be explained by possible concentration and pH gradients during the

leaching process. The formation of the layer appears to occur via a competitive growth and dissolution process of aluminium hydroxide at the aluminium interface as suggested by Tabrizi *et al.*[41] Oxide layers with a dual morphology were generated on aluminium, consisting of an inner barrier layer and an outer non-barrier crystalline layer, in long-term exposure to alkaline media. Similar layers were observed when aluminium was subjected to weak alkaline conditions by Hurlen and Haug.[42] The thickness of the barrier layer was decreasing with increasing pH. Considering the relatively thick dense inner layer, it can be assumed that the formation of the protective layer from these lithium-based organic coatings occurs at weak alkaline pH. In addition to this process, the role of lithium needs to be considered.

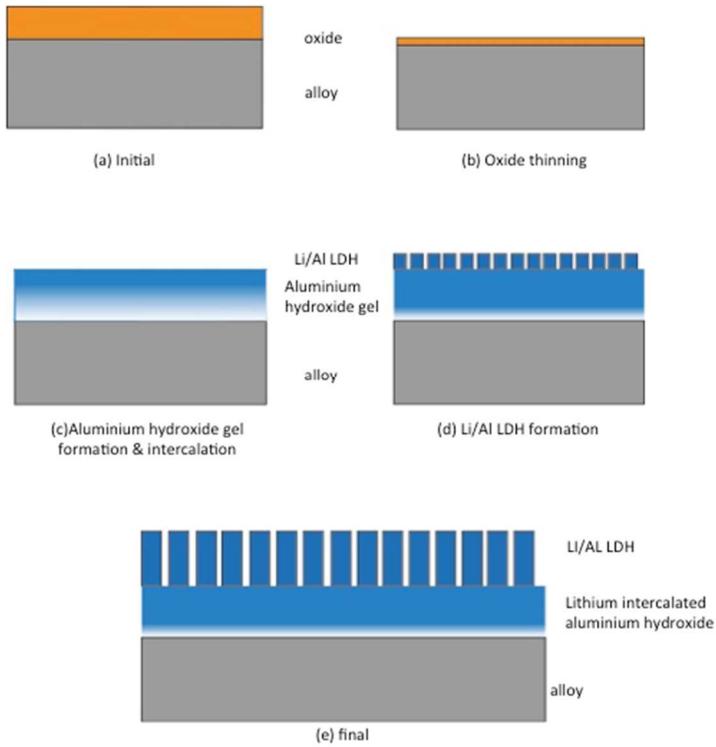

Fig. 12. Schematic illustration of the steps in the formation.

The proposed mechanism of layer formation consists of several processes (Fig. 12). First, oxide thinning will occur due to chloride-ion adsorption in the oxide layer[39] when the aluminium is exposed to the sodium chloride solution of the salt spray test. At the same time, the leaching process starts and lithium-salts will be released from the organic coating matrix. Both lithium carbonate and lithium oxalate have an alkaline nature in solution. In addition to this, the magnesium oxide in the coating can act as an alkaline buffer and will provide an alkaline pH in the bulk solution. Since there are no significant amounts of magnesium found in the

elemental analysis, it can be assumed that magnesium is not active in the inhibition process.

The second process is the destabilisation of the hydrated aluminium oxide in the alkaline chloride-containing environment. This process transfers the initial hydrated aluminium oxide into an aluminium hydroxide gel at the surface. Once the oxide layer is sufficiently thinned, the corrosion process commences via the direct attack and dissolution of the aluminium. In this alkaline chloride-containing environment, the Al^{3+} ion hydrolyses and forms amorphous $Al(OH)_3$ at the aluminium substrate interface (growth process).[40]

The third process is the dissolution reaction of the aluminium hydroxide gel at the oxide electrolyte interface. The aluminium hydroxide gel that was formed in the second process will dissolve into ionic $Al(OH)_4^-$ at the aluminium hydroxide gel / electrolyte interface (dissolution process). $Al(OH)_4^-$ is the main species present in alkaline environment.[44, 45] The equilibrium or dissolution rate depends on the pH.[46] Therefore, at high pH, the solubility of $Al(OH)_4^-$ is high and it is expected that the aluminium hydroxide gel will be thin.

The SEM results show the formation of a dense layer in the early stages of salt spray exposure. In addition, EELS data reveal the presence of lithium in the dense barrier layer. Rangel and Travassos [34] suggest formation of lithium aluminate ($LiAlO_2$) via the AlO_2^- ion. However, this seems unlikely since this dehydrated form of $Al(OH)_4^-$ does not exist in significant concentrations according to Sipos[45]. The Lithium ion is known for its facile intercalation into aluminium hydroxides, such as Bayerite and Gibbsite, forming Layered double hydroxides (LDH).[47] Moreover, amorphous aluminium hydroxides are known as effective sorbents of lithium salts[48]. Therefore, it can be assumed that lithium intercalates with the aluminium hydroxide gel to generate very small grain size particles or even an amorphous structure resulting in a dense impermeable protective layer.

The fourth process is the formation of the non-barrier outer layer. It is still unclear whether this step is a precipitation reaction of or an aging process from the hydroxide gel process. It is assumed that $Al(OH)_4^-$ dissolves from the outer side of the aluminium hydroxide gel forming a Li/Al layered double hydroxide from the reaction between $Al(OH)_4^-$ and Li^+. The SEM cross-sectional results suggest that the precipitation or aging reaction occurs at a later stage in the formation of the protective layer. Process 3 and 4 (growth and dissolution) are in competition with each other. However, these processes terminate when the dense layer is thick and dense enough and does not allow any Al^{3+} of Li^+ diffusion. At this stage the inhibition process is complete.

4. Conclusions

Lithium-containing salts were used as leachable corrosion inhibitors in model organic coatings for the protection of AA2024-T3 aluminium alloys. These lithium salt loaded coatings demonstrated effective corrosion inhibition when exposed to corrosive conditions like neutral salt spray (ASTM B-117) for 168 hours, providing clean scribes with no corrosion products. TEM-EELS and SEM cross-sectional analysis of the scribed area revealed that lithium ions were leached from the coating matrix and formed a protective layer on the 2024-T3 aluminium alloy of the scribed area, which protected the alloy from corrosion. The thickness of the layer varied, ranging from 0.5-1.5 µm. The general morphology of the protective layer salts

showed three distinct regions, comprising a dense barrier layer near the metal/passive layer interface, a porous layer in the middle, and an outer columnar layer. The layer comprised aluminium, oxygen and lithium, as identified by EELS analysis and lithium was relatively uniform distributed in the layer. The poly-crystalline outer layer could be an Al/Li layered double hydroxide. The dense barrier layer is composed of lithium and aluminium hydroxide. However, it remains unclear in which form. The formation of this layer is a multistep process controlled by competitive film growth and dissolution processes.

5. Acknowledgments.

The authors would like to thank Dr. Simon Gibbon and Gerard Smyth for their support and contributions. Dr. Derek Graham for the white light interferometry, and Dr.Yaiza Gonzalez Garcia. This work was performed under the collaboration agreements of AkzoNobel with The University of Manchester and Delft University of Technology.

6. References

1. R. L. Twite and G. P. Bierwagen, *Progress in Organic Coatings*, 1998, 33, 91-100.
2. N. Birbilis and R. G. Buchheit, *Journal of the Electrochemical Society*, 2005, 152, B140-B151.
3. R. G. Buchheit, R. P. Grant, P. F. Hlava, B. McKenzie and G. L. Zender, *Journal of the Electrochemical Society*, 1997, 144, 2621-2628.
4. A. Boag, A. E. Hughes, A. M. Glenn, T. H. Muster and D. McCulloch, *Corrosion Science*, 2011, 53, 17-26.
5. A. E. Hughes, R. J. Taylor, K. J. H. Nelson, B. R. W. Hinton and L. Wilson, *Mater. Sci. Technol.*, 1996, 12, 928-936.
6. M. Kendig, S. Jeanjaquet, R. Addison and J. Waldrop, *Surface and Coatings Technology*, 2001, 140, 58-66.
7. D. Chidambaram, C. R. Clayton, M. W. Kendig and G. P. Halada, *Journal of the Electrochemical Society*, 2004, 151, B613-B620.
8. S. J. Garcia-Vergara, P. Skeldon, G. E. Thompson and H. Habazaki, *Surface and Interface Analysis*, 2007, 39, 860-864.
9. J. Sinko, *Progress in Organic Coatings*, 2001, 42, 267-282.
10. L. Xia, E. Akiyama, G. Frankel and R. McCreery, *Journal of the Electrochemical Society*, 2000, 147, 2556-2562.
11. F. H. Scholes, S. A. Furman, A. E. Hughes, T. Nikpour, N. Wright, P. R. Curtis, C. M. Macrae, S. Intem and A. J. Hill, *Progress in Organic Coatings*, 2006, 56, 23-32.
12. M. W. Kendig and R. G. Buchheit, *Corrosion*, 2003, 59, 379-400.
13. H. Wang, F. Presuel and R. G. Kelly, *Electrochimica Acta*, 2004, 49, 239-255.
14. S. A. Furman, F. H. Scholes, A. E. Hughes and D. Lau, *Progress in Organic Coatings*, 2006, 56, 33-38.
15. O. Lopez-Garrity and G. S. Frankel, *Journal of the Electrochemical Society*, 2014, 161, C95-C106.
16. M. Iannuzzi, T. Young and G. S. Frankel, *Journal of the Electrochemical Society*, 2006, 153, B533-B541.
17. R. L. Cook Jr, *Corrosion*, 2000, 56, 321-333.

18. A. E. Hughes, J. D. Gorman, T. G. Harvey, A. Galassi and G. McAdam, *Corrosion*, 2006, 62, 773-780.
19. J. A. Hill, T. Markley, M. Forsyth, P. C. Howlett and B. R. W. Hinton, *Journal of Alloys and Compounds*, 2011, 509, 1683-1690.
20. D. Ho, N. Brack, J. Scully, T. Markley, M. Forsyth and B. Hinton, *Journal of the Electrochemical Society*, 2006, 153, B392-B401.
21. T. Stimpfling, F. Leroux and H. Hintze-Bruening, *European Journal of Inorganic Chemistry*, 2012, 2012, 5396-5404.
22. M. Forsyth, M. Seter, M. Y. Tan and B. Hinton, *Corrosion Engineering Science and Technology*, 2014, 49, 130-135.
23. A. J. Aldykewicz, Jr., H. S. Isaacs and A. J. Davenport, *Journal of the Electrochemical Society*, 1995, 142, 3342-3350.
24. M. O'Keefe, B. Fahrenholtz, E. Morris and R. Albers, Chicago, IL, 2013.
25. M. E. Nanna and G. P. Bierwagen, *Jct Research*, 2004, 1, 69-80.
26. P. Plagemann, J. Weise and A. Zockoll, *Progress in Organic Coatings*, 2013, 76, 616-625.
27. S. V. Lamaka, M. L. Zheludkevich, K. A. Yasakau, M. F. Montemor and M. G. S. Ferreira, *Electrochimica Acta*, 2007, 52, 7231-7247.
28. M. L. Zheludkevich, K. A. Yasakau, S. K. Poznyak and M. G. S. Ferreira, *Corrosion Science*, 2005, 47, 3368-3383.
29. T. G. Harvey, S. G. Hardin, A. E. Hughes, T. H. Muster, P. A. White, T. A. Markley, P. A. Corrigan, J. Mardel, S. J. Garcia, J. M. C. Mol and A. M. Glenn, *Corrosion Science*, 2011, 53, 2184-2190.
30. G. Bierwagen, R. Brown, D. Battocchi and S. Hayes, *Progress in Organic Coatings*, 2010, 67, 195-208.
31. WO2010112605-A1; AU2010230147-A1; KR2012007506-A; US2012025142-A1; EP2414464-A1; CN102378793-A; IN201106820-P4; EP2414464-B1; RU2011144574-A, 2010.
32. J. Gui and T. M. Devine, *Scripta Metallurgica*, 1987, 21, 853-857.
33. C. M. Rangel and M. A. Travassos, *Corrosion Science*, 1992, 33, 327-343.
34. C. M. Rangel, Travassos, M.A. , *Surface & coatings technology*, 2006, 200, 5823-5828.
35. R. G. Buchheit, Bode, M.D., Stoner, G.E., *Corrosion*, 1994, 50, 205-214.
36. C. A. Drewien, Eatough, M.O., Tallant, D.R., Hills, C.R., Buchheit, R.G., *Journal of material research*, 1996, 11, 1507-1513.
37. M. R. S. Castro, J. C. Nogueira, G. P. Thim and M. A. S. Oliveira, *Thin Solid Films*, 2004, 457, 307-312.
38. M. Frenkel, A. Glasner and S. Sarig, *The Journal of Physical Chemistry*, 1980, 84, 507-510.
39. R. T. Foley, *Corrosion*, 1986, 42, 277-288.
40. R. T. Foley and T. H. Nguyen, *Journal of The Electrochemical Society*, 1982, 129, 464-467.
41. M. R. Tabrizi, S. B. Lyon, G. E. Thompson and J. M. Ferguson, *Corrosion Science*, 1991, 32, 733-742.
42. T. Hurlen and A. T. Haug, *Electrochimica Acta*, 1984, 29, 1133-1138.
43. P. Visser, Chicago, IL, 2013.
44. L. A. Carreiea, V. A. Maroni, J. W. Swaine Jr and R. C. Plumb, *The Journal of Chemical Physics*, 1966, 45, 2216-2220.
45. P. Sipos, *Journal of Molecular Liquids*, 2009, 146, 1-14.
46. C. F. Baes and R. E. Mesmer, *The hydrolysis of cations*, Wiley, 1976.
47. G. R. Williams and D. O'Hare, *J Phys Chem B*, 2006, 110, 10619-10629.
48. V. P. Isupov, *Journal of Structural Chemistry*, 1999, 40, 672-685.